Solving the Stellar Structure Equations for Main Sequence Stars with MESA

Austin Scott, Bellarmine College Preparatory, austin.g.scott26@gmail.com

Acknowledgements

Thank you for the guidance of Shahed Shayan-arani, a UCSD PhD student, in the development of this research paper.

Abstract

The structure and evolution of stars are managed by a small set of physical principles that can be expressed through the four fundamental equations of stellar structure: hydrostatic equilibrium, mass continuity, energy conservation, and energy transport. Together with the equation of state, energy generation processes, and opacity, these equations describe how a star maintains balance between self-gravity, internal pressure, and energy output. Furthermore, nuclear processes (for example, the CNO cycle or proton–proton chain) determine how stars evolve and generate energy over time. Using these basic frameworks, the relations between different features of stars, such as mass or luminosity, can be visualized using various plots, most notably, the Hertzsprung-Russell diagrams.

The equations of stability and evolution of main sequence stars are usually impossible to solve by hand; however, using the Modules for Experiments in Stellar Astrophysics (MESA) framework interfaced from Python, these equations can be solved. MESA generates detailed outputs regarding composition, luminosity, and many other factors, allowing for simulations of main sequence stars with varying initial conditions. I focused on the effect on aspects such as metallicity, temperature, and density, and compared the results to theoretical expectations. The four simulations I ran using varying mass sizes typical of main sequence stars aligned closely with theory. These results demonstrate how stellar structure theory and numerical modeling together replicate main sequence stellar evolution.

Solving the Stellar Structure Equations for Main Sequence Stars with MESA

Introduction

A star is generally defined by two conditions: the first being that it is bound by self gravity; and the second being that it radiates energy from an internal source (usually nuclear fusion). A comet or planet, by definition, is thus not a star because it does not radiate energy from an internal source. From these parameters, multiple assumptions can be made for stellar modeling but these will be explained in the following section. Unlike other forms of physical science, direct experimentation is relatively impossible to perform on stars, leading to the reliance on observation to support theories. The primary characteristics to be measured are the luminosity and the general shape of its spectrum, which allows inferences on effective temperature, chemical composition, mass, and radius. Although these properties are observable, they do not match the full complexity of the internal structure of a star or explain how stars maintain stability throughout their lifetimes. Therefore, we require a theoretical framework to pursue these understandings. This framework relies on a set of physical laws, expressed as the fundamental equations of stellar structure: hydrostatic equilibrium, mass continuity, energy conservation, and energy transport. Combined with the relations between the equation of state, energy generation, and opacity, this framework allows us to predict the internal structure and evolution of stars.

Since stars cannot be reproduced in laboratory experiments, these models contain the only methods for connecting observable properties to physical principles. However, these equations are virtually impossible to solve analytically for realistic conditions. As a result, numerical modeling approaches have become essential for this task. Computational frameworks have been developed that can solve the equations of stellar structure, evolution, and composition. I used Modules for Experiments in Stellar Astrophysics (MESA) to produce models that can be directly compared with theoretical expectations. I chose to focus on main-sequence stars as the focus of this study because they represent the longest lived and most stable phase of stellar evolution. It also allows for the most direct comparison between theory and the models as main sequence stars avoid many of the complications of later evolutionary stages, such as strong mass loss or shell burning, while still representing the essential physics of stellar structure. With these models, I seek to test whether the theoretical predictions from these equations match the data generated by numerical models (MESA).

Background

Fundamental Equations of Stellar Structure

As stated earlier, there are four fundamental equations of stellar structure. However, these tenets rely on three main, basic assumptions regarding the structure of stars: isolation, uniform initial composition, and spherical symmetry. First, the isolation assumption considers every star as isolated in space, even though it must invariably be part of a larger group–a galaxy. This assumption allows the initial conditions to exclusively determine the course of the star's evolution. Second, the uniform initial composition assumption presumes that stars are born with a given mass and seemingly given, homogenous composition. Hydrogen and helium are the predominant stellar components, and each are found as a gas save for extremely low

temperatures or extremely high pressures; thus, stars are deduced to consist of gas. Third, the spherical symmetry assumption supposes every star to be evaluated as a perfect sphere. Therefore, the physical properties within a star will change only with the change in radial distance from the center, and are uniform over a spherical surface of the same radius (the spatial variable for radius can also be replaced by enclosed mass). From these assumptions, structure can be expressed from the aforementioned four traditional differential equations.

The first equation is the equation for mass continuity, which defines the mass m enclosed within radius r. The transformation between these variables is given in terms of density ρ.

$$m(r) = \int_0^r 4\pi r^2 \rho(r) dr$$

It can also be written in differential form:

$$dm = \rho 4\pi r^2 dr$$

Essentially, this equation depicts $m(r)$, the total mass within the sphere of radius r, and how for each increase of r by dr, the additional mass is equal to the volume of a thin shell $4\pi r^2 dr$ times the local density ρ.

The second equation is the equation of motion and describes the state of hydrostatic equilibrium. Pressure is defined by P and G is the gravitational constant.

$$\frac{dP}{dm} = -\frac{Gm}{4\pi r^4}$$

Or, by dividing by dm/dr:

$$\frac{dP}{dr} = -\rho\frac{Gm}{r^2}$$

This equation describes how the rate at which pressure decreases as the radius increases balances the inward pull of gravity. These two forms are equivalent, but the version expressed in terms of m is useful for numerical modeling, while the r form is more intuitive for describing pressure balance with depth.

The third equation regards energy generation, effectively how much energy is produced inside the given star. In the equation, L represents luminosity, $4\pi\rho r^2$ gives the mass of the shell, and ϵ tells the energy generation per unit mass.

$$\frac{dL}{dr} = 4\pi\rho r^2\varepsilon$$

Effectively, $\frac{dL}{dr}$ solves for how much energy is added via nuclear reactions in thin shells as r increases. However, if the shell loses energy (such as neutrinos escaping), those must be subtracted from this value as well.

The fourth equation is the equation of energy transport. There are two forms of this equation based on how the energy moves: radiative and convective. In the below equation for radiative energy transport, T is local temperature, κ is opacity, a is the radiation constant, c is the speed of light, and ρ is density.

(Radiative)

$$\frac{dT}{dr} = -\frac{3\kappa\rho L}{16\pi acT^3 r^2}$$

This equation relates changes in temperature by radius with luminosity and opacity. It shows that a higher luminosity or opacity leads to a steeper temperature gradient.

However, using the Schwarzschild criterion, convection occurs when $\nabla_{rad} > \nabla_{ad}$ (All modeling trials used MESA's default, the Schwarzschild criterion). When convective energy transport occurs, the energy is carried by the bulk motion of the gas rather than the photons. In this case, the temperature gradient adjusts to the adiabatic temperature gradient, which depends on the properties of the gas. In this equation, P is the pressure, $\frac{dP}{dr}$ is given by the hydrostatic equilibrium equation, and $\frac{d\ ln(T)}{d\ ln(P)}$ represents the adiabatic temperature gradient.

(Convective)

$$\left(\frac{dT}{dr}\right)_a = \frac{T}{P}\left(\frac{d\ ln(T)}{d\ ln(P)}\right)\frac{dP}{dr}$$

In regions where convection dominates, the temperature gradient is nearly adiabatic because convection efficiently transports energy with minimal temperature difference.

Along with these fundamental equations, proper timescales are necessary to effectively model stellar evolution. There are three main basic timescales: the dynamical timescale, the thermal timescale, and the nuclear timescale.

The dynamical timescale:

$$T \sim \sqrt{\frac{R^3}{GM}}$$

This timescale roughly measures the time over which hydrostatic balance is restored. In other words, how long it would take a star to collapse or expand if pressure support instantly vanished. For reference, the dynamical timescale of the Sun is about 1000 seconds ($T_{dyn,\odot} \approx 1.6 \times 10^3$). This timescale is extremely short, only measuring that dynamical process; of which, each end state–collapse, explosion, or restoration of hydrostatic equilibrium–will occur within a period of time of the order of the dynamical timescale. As a result, stars may be assumed to be in a state of hydrostatic equilibrium, as any change to this state is immediately resolved. Regardless, stars are not static during their entire lifespan, and thus, they evolve *quasi-statically,* constantly adjusting their internal structure so as to maintain dynamical balance. If the star fails to maintain its dynamical balance, the imminent collapse or explosion is observable in its entirety. These events are known as *supernovae*.

The thermal timescale:

$$T \sim \frac{GM^2}{RL}$$

The thermal timescale is significantly longer than the dynamical timescale yet still only represents a sliver of the lifespan of a star. Therefore, we cannot observe the development of a thermal process in a star yet may still assume that throughout most of its life a star is in a state of thermal equilibrium. The thermal timescale reflects the time it would take for a star to emit all of its stored heat (gravitational and thermal energy) if nuclear fusion stopped, provided it maintains

a constant luminosity. For reference, the thermal timescale of the sun is roughly 30 million years ($T_{th,\odot} \approx 3.1 \times 10^7$).

The nuclear timescale:

$$T \sim \frac{f \varepsilon M c^2}{L}$$

The nuclear timescale is the longest timescale of the three by far. Here, c is the speed of light, ε is the efficiency of the nuclear fusion process, and f is the fraction of the star's total mass that is available to be used as nuclear fuel. For example, the nuclear timescale for the Sun is comparable to the Sun's expected main-sequence lifetime and to the estimated age of the universe at the same order of magnitude. This timescale essentially tracks the actual lifetime for burning available nuclear fuel, and it sets main-sequence lifetimes. The length of this timescale indicates that stars seem to have actually consumed only a small fraction of their available nuclear energy. In essence, only a tiny portion of the stellar mass has changed its initial composition. Another conclusion is that nuclear equilibrium is simply not to be expected.

The hierarchy of $T_{dyn} \ll T_{th} \ll T_{nuc}$ justifies the quasi-static evolutionary modeling in which hydrostatic equilibrium is maintained while the structure slowly changes over the nuclear timescales. From this, simply knowing the initial composition, which is assumed as uniformly distributed throughout the star, allows for tracing the evolution of stars.

The nuclear timescale also explains why higher mass stars have shorter lifespans than stars of lower masses. A star's luminosity roughly follows this mass-luminosity relation on the main sequence for mid-range masses:

$$L \propto M^{3.5}$$

Since the amount of available fuel to a star is proportional to a star's mass, the nuclear timescale can be written as:

$$T_{nuc} \propto \frac{M}{L} \propto M^{-2.5}$$

Thus, although high-mass stars contain more fuel, they burn it at a significantly faster rate. Consequently, massive stars live only a few million years, while low-mass stars can persist for billions of years.

To fully determine the hydrostatic equilibrium equation, and determine how a star responds to compression, heating, or cooling, an equation of state (EOS) is needed. The EOS provides the necessary connection between the stellar structure equations, linking the thermodynamic variables in the star's interior. At a base level, an equation of state relates the pressure P exerted by a system of particles of known composition, to density ρ, ambient temperature T, and chemical makeup (mass fractions of hydrogen, helium, and heavier elements). In stars, this relationship is vital because pressure can arise from multiple physical sources.

For a fully ionized plasma, the dominant contribution is ideal gas pressure:

$$P = \frac{\rho k T}{\mu m_H}$$

In this equation, μ denotes the mean molecular weight (which depends on composition), while m_H denotes the mass of a hydrogen atom. In low and intermediate mass main sequence stars, this pressure is dominant.

At higher temperatures, radiation pressure contributes significantly:

$$P_{rad} = \frac{1}{3} aT^4$$

In this equation, a is the radiation constant. Radiation pressure arises from the momentum that is transferred to gas particles from photons whenever they are absorbed or scattered. In massive stars, radiation pressure can rival or even exceed gas pressure, altering stability.

Additionally, there is a third main source of pressure, the equation of state for *degeneracy pressure* (or *electron pressure*). The degeneracy pressure is generated by electrons that are forced into higher momentum states as their density increases. Below is the proportionality for ideal degenerate electron gas.

For the non-relativistic case:

$$P \propto \rho^{5/3}$$

For the relativistic case:

$$P \propto \rho^{4/3}$$

In main sequence stars, this pressure is negligible, but in compact objects such as neutron stars it plays a much larger role.

As a whole, equations of state govern pressure and temperature. It is central to stellar structure because it determines how pressure is built up from gas particles, photons, and in extreme cases, degenerate electrons. By relating pressure with multiple other factors such as composition and temperature, it determines not only the balance of forces within a star, but also how compressibility, stability, and heat capacity behave, directly influencing hydrostatic equilibrium. For realistic stellar modeling, EOS treatments must capture not only the contributions of ideal gas and radiation pressure, but also include additions such as degeneracy and partial ionization. For this reason, modern stellar modeling models like MESA rely on detailed EOS tables to accurately describe conditions across all regions of a star.

One of the major tools for evaluating the evolution of stars is the Herzsprung–Russell Diagram (also known as H–R Diagrams). These plots relate the two most fundamental properties of a star that can be inferred from observation: luminosity L and effective temperature T_{eff}. The x-axis, decreasing rightward, displays T_{eff} while the y-axis displays L. Because of the relations between luminosity and mass, and temperature and radius, H–R diagrams can loosely be understood as having relative mass on the y-axis and radius on the x-axis. Only certain combinations of L and T_{eff} values are possible, with the majority of points found along a narrow strip that runs diagonally through the diagram. This strip is known as the *main sequence*, and thus the stars in it are known as *main-sequence stars*. The other two main regions are the *red giant* stars (found upwards and to the right of the *main sequence*) and *white dwarf* stars (found below and to the left of the *main sequence*).

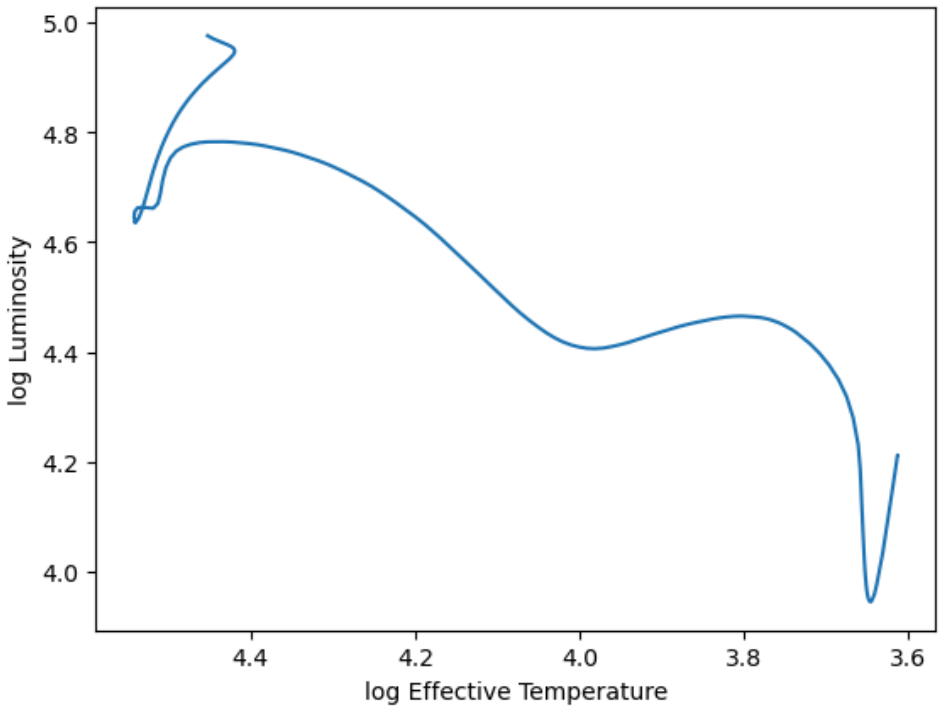

Figure 1. Included above is a Hertzsprung-Russell evolution diagram of a 20 $M_{\odot}$ star. The x-axis corresponds to $log\ T_{eff}$ and the y-axis corresponds to $log\ L$.

All together, these theoretical frameworks for stellar structure, from the basic assumptions, to the four fundamental equations, to the three main timescales, and finally to the equation of state, provide predictions that can be tested against stellar models. Although analytic theory provides these insights, the underlying equations are tightly coupled and highly nonlinear. Hydrostatic equilibrium requires knowledge of pressure, but the pressure itself depends on the equation of state, which in turn depends on temperature, density, and composition. Nuclear energy generation depends on temperature, feeding back into the luminosity and structure of the star. Opacity determines composition and temperature and directly influences energy transport, which then determines whether a region is stable against convection. Because of these interdependencies, solving the stellar structure equations in a realistic way is impossible by hand.

For this reason, numerical simulations have become essential to modern stellar astrophysics. Computational frameworks such as the *Modules for Experiments in Stellar Astrophysics (MESA)* allow these equations to be solved simultaneously with detailed microphysics, including nuclear reaction networks and realistic equations of state. MESA's outputs (which include luminosity, effective temperature, composition profiles, etc.) can then be directly compared with the predictions of stellar structure theory. In this project, I use MESA simulations of main-sequence stars with varying masses to test whether the results align with the theoretical expectations outlined above.

The MESA Framework

MESA (*Modules for Experiments in Stellar Astrophysics*), as stated previously, is the computational framework I have used for this project. As a one-dimensional, open-source advanced stellar evolution code, MESA blends both numerical and physical modules to create simulations for a wide array of stellar scenarios. To model these stars, MESA solves the coupled equations of structure and composition simultaneously. MESA's widespread use can be attributed to its flexible and straightforward use because of its modular design; its easy accessibility because of its open-source nature; its wealth of online resources and references online; and its wide range of capabilities from its intense customizability of both age and mass.

The framework takes inputs through various *inlist* files where the specified outputs, initial conditions, and other variable controls are defined. Some of these variables include metallicity or mass whereas other controls in the files regard additional properties such as wind, rotation, or atmosphere. For the purposes of this study however, I focused only on the comparison of stars of differing initial masses. The outputs are stored in *profile* and *history* files,

where profile files contain detailed information about saved models at specific timesteps and history files hold the general trends of stellar properties over the entire lifespan. The data contained within these files can then be compiled into graphs and diagrams for understanding the course of a star's life.

For this paper, I conducted four evolutionary trials total, with each run containing the exact same initial conditions except for mass which varied between runs. I used MESA version r24.08.1 compiled with fortran build 13.3.0. I chose to also focus only on the main sequence part of each star's lifespan to compare with one another. The four initial masses I used were: 1 $M_{\odot}$, 5 $M_{\odot}$, 10 $M_{\odot}$, and 15 $M_{\odot}$. I chose these masses because it gave a sufficient range of common mass stars, from those similar to our sun to those many times larger. I began each with a simple pre-main sequence model, with an initial metallicity mass fraction of 0.02, and absent of wind and element diffusion. MESA internally computed initial Y from the enrichment law $Y = 0.24 + 2Z$, therefore initial $Y = 0.28$ and initial $X = 0.70$ since $X = 1 - Y - Z$. Only standard convective mixing was active, and MESA's default simple photosphere atmosphere was used for all four trials. I saved one history file per run, and recorded profiles every fifty timesteps. I stopped each run once the center mass fraction of H dropped below 1d-3.

Parameter	Value	Source (inlist_project)
Initial Mass	$1, 5, 10, 15\ M_{\odot}$	`initial_mass=1`
Initial metallicity Z	0.02	`initial_z=0.02`
Type II Opacities	Enabled, Zbase=0.02	`use_Type2_opacities=.true.`
Pre-main-sequence start	Yes	`create_pre_main_sequence_model=.true.`

Stop criterion	Central H $X_c(H^1) < 10^{-3}$	`xa_central_lower_limit_species(1)='h1'` `xa_central_lower_limit(1)=1d-3`
Energy equation/tolerances	Debt, gold tolerances enabled	`energy_eqn_option='dedt'` `use_gold_tolerances=.true.`
Output Cadence	History every model; profile every 50 models	`history_interval=1` `profile_interval=50`
Other model physics	Left at MESA r24.08.1 defaults	
MESA Release	r24.08.1	

Table 1. Summary of the primary MESA input parameters used for all runs. Only quantities explicitly changed from default MESA r24.08.1 values are listed. Each model began from a pre-main-sequence configuration and was evolved until the central hydrogen mass fraction dropped below 10^{-3}.

All parameters not explicitly listed were left at their default values for MESA r24.08.1. In my history and profile files, I recorded the major characteristics of the stars such as luminosity, mass, radius, metallicity, effective temperature, density, etc. I then used mesareader in Python to create basic plots using these data values from the history or profile data. In the next section, I will present these results and evaluate how reflective these outcomes are of theoretical predictions.

Results

I have simulated stellar evolution for four different initial masses: 1, 5, 10, and 15 $M_\odot$ and examined their evolutionary track and internal structure. The following plots include Hertzsprung-Russell diagrams and density vs radius, effective temperature vs radius, and metallicity evolution profiles for each mass. These results are compared with theoretical expectations from stellar theory.

Hertzsprung-Russell Diagrams

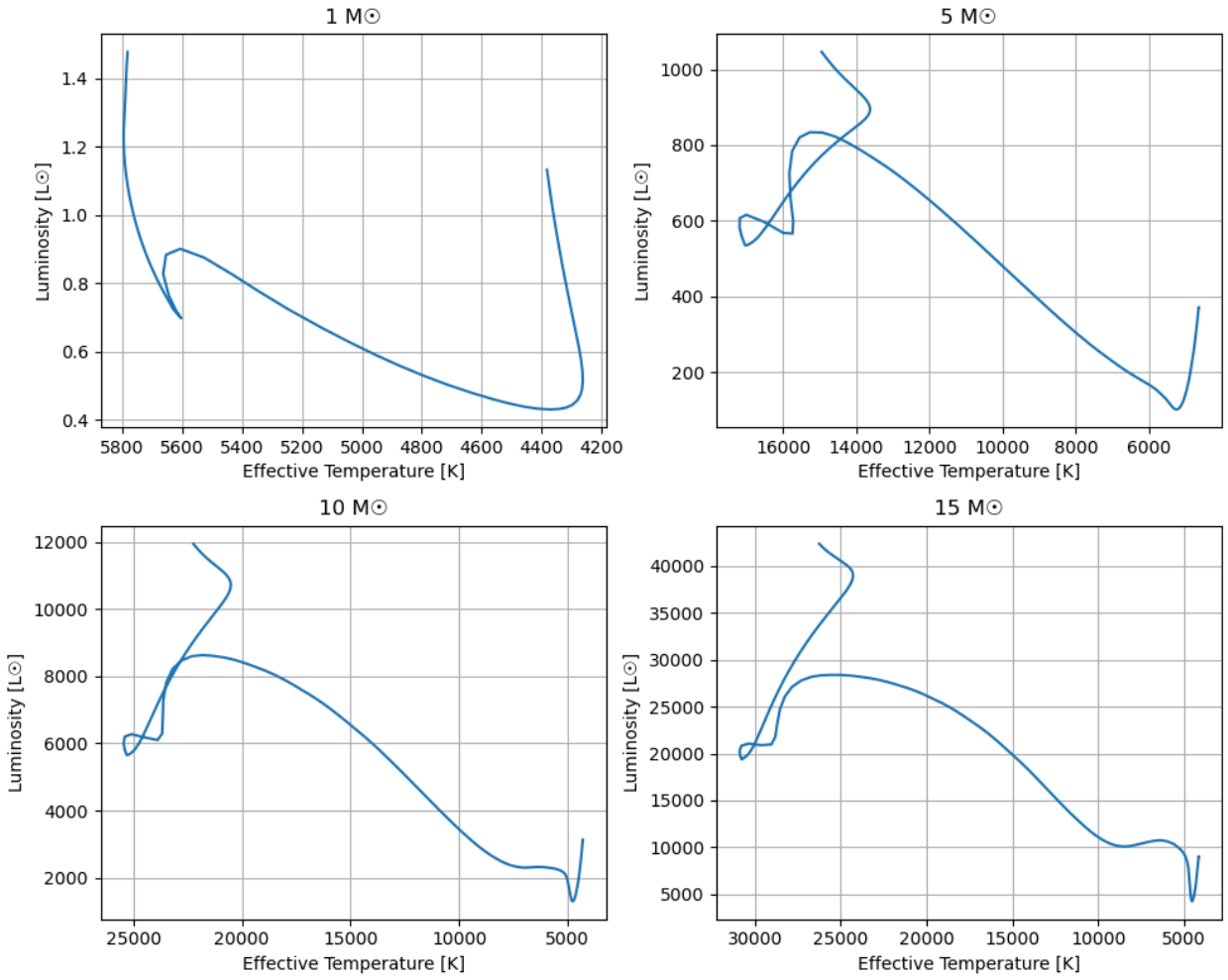

Figure 2. Evolutionary tracks in the Hertzsprung–Russell diagram for main-sequence stars of initial masses 1 $M_{\odot}$, 5 $M_{\odot}$, 10 $M_{\odot}$, and 15 $M_{\odot}$. Each track shows luminosity L versus effective temperature T_{eff}. Higher-mass models are hotter and more luminous, following the theoretical mass-luminosity relation and displaying characteristic main-sequence "hooks" near hydrogen exhaustion.

The most obvious trend from these plots simply corresponds the mass of a star to effective temperature and luminosity. For example, the 1 $M_{\odot}$ star model reaches a rough maximum effective temperature of 5800 K, with a luminosity that peaks around 1.5 $L_{\odot}$. On the contrary, the 15 $M_{\odot}$ star reaches significantly higher values for both these factors–more than

$30000\ K$ and $40000\ L_{\odot}$ for effective temperature and luminosity respectively. This general tendency matches with the theoretical predictions that expect this relationship.

Furthermore, the smaller mass stars of 1 $M_{\odot}$ and 5 $M_{\odot}$ retain much stabler evolution tracks as compared with the larger mass stars, which contain prominent loops and hooks. The 1 $M_{\odot}$ track begins near solar values and slowly increases in luminosity over the main sequence, consistent with steady p–p burning in a radiative core. The 5 $M_{\odot}$ track is hotter and more luminous, reflecting its convective core, and has a shorter main sequence which ends in a hook-like shape as hydrogen is exhausted. Both the 10 $M_{\odot}$ and 15 $M_{\odot}$ are much more luminous and hot than the smaller mass stars, becoming nearly horizontal throughout the main sequence, which reflects the CNO cycle and radiation pressure support in their convective cores. The small "hooks" at the bottom right of the diagrams, near the end of the main sequence, are caused by the end of the main sequence and exhaustion of hydrogen burning, as the stars start towards burning helium. Thus, these H–R diagrams, of the four MESA simulations, reproduced the expected trends across mass ranges.

The results from the density and radius diagrams also provide similar results:

Density and Radius Plots

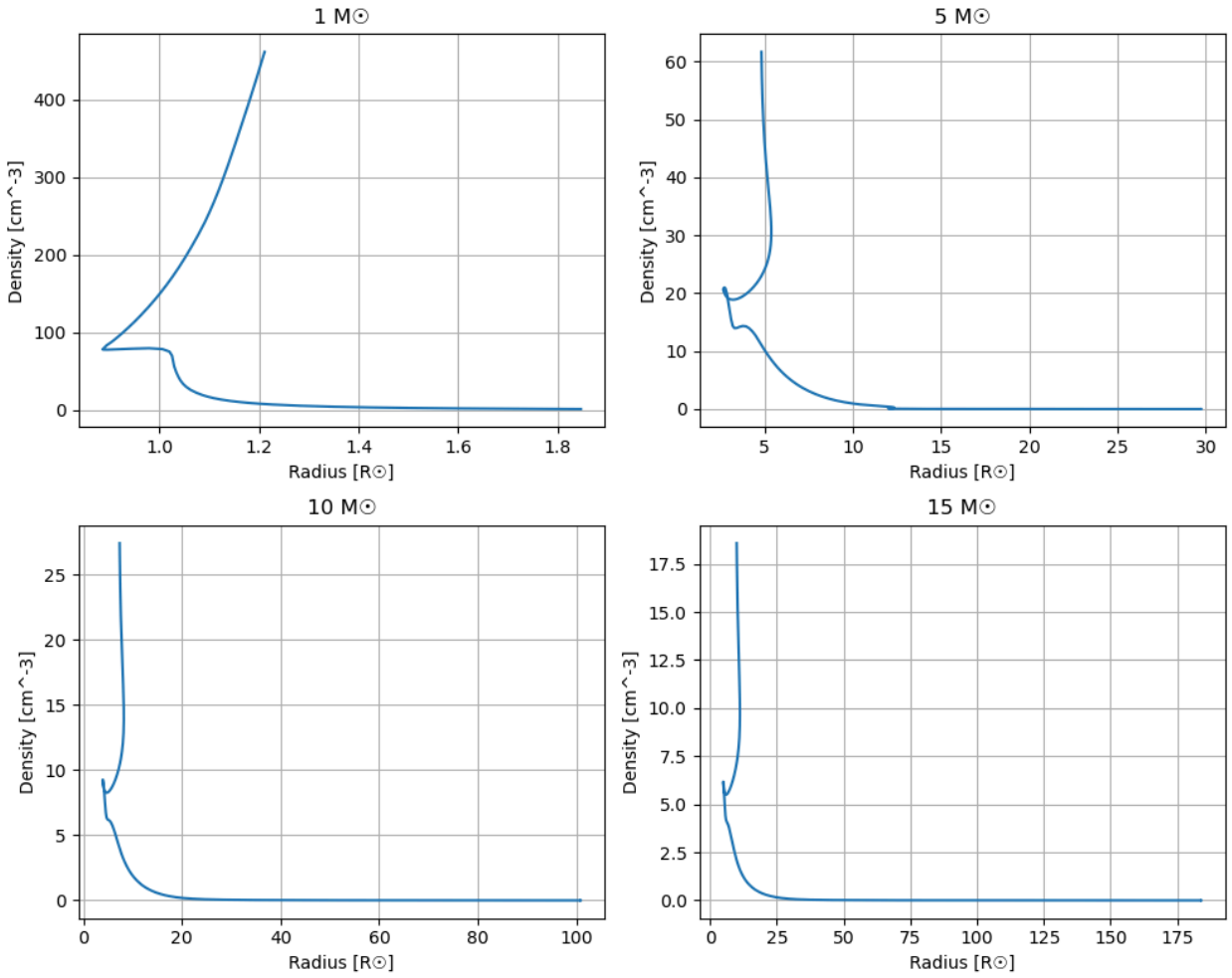

Figure 3. Radial density profiles for models of 1 $M_\odot$, 5 $M_\odot$, 10 $M_\odot$, and 15 $M_\odot$. Low-mass stars show sharply peaked central densities associated with radiative cores, whereas higher-mass models develop extended, flatter cores due to convective mixing. The overall decrease in mean density with increasing stellar mass follows the $\rho \sim \frac{M}{R^3}$ scaling from the mass-continuity equation.

Here, the most immediate observation regards the scaling of the plots for each of the trials. The smallest mass star of 1 $M_\odot$ reflects maximum densities significantly greater than the 15 $M_\odot$ and 10 $M_\odot$ stars, and still more than six times greater than even the 5 $M_\odot$ star (~450 g/cm^3 compared to ~60 g/cm^3). The radii of the four stars reflect this trend as well, as the larger mass stars of 10 $M_\odot$ and 15 $M_\odot$ reach much larger radii (between roughly 100-200 $R_\odot$)

than the both the 1 $M_\odot$ and 5 $M_\odot$ stars which never exceed 2 $R_\odot$ and 30 $R_\odot$ respectively. Combined, these two factors explain how larger mass stars swell to exponentially larger sizes with significantly lower density throughout, as compared with smaller mass stars. Returning to theory, the equation for mass continuity matches these observations. By assuming a uniform mass (to gain a general estimate) and solving for ρ, the equation yields a rough approximation where $\rho \sim \frac{M}{R^3}$. As compared with the plots, this explains why the 10 $M_\odot$ and 15 $M_\odot$ stars, which develop radii between 100-200 $R_\odot$, have envelopes with densities orders of magnitudes smaller than the 1 $M_\odot$ star. This relation also explains why the density falls off more gradually in higher-mass stars, as spreading the same mass over a greater radius and thus volume produces lower and less sharply peaked density profiles.

The shapes of the tracks in the diagrams also reveal trends that match expected results. In the 1 $M_\odot$ star, the density drops rapidly past 1 $R_\odot$, indicating extremely high central density. In the 5 $M_\odot$, 10 $M_\odot$, and 15 $M_\odot$ stars, the density also drops near the outer core, but in a much less steep way. These observations reflect the types of cores that stars of lower and higher masses form. Since the lower mass star of 1 $M_\odot$ transports energy via radiation (thus having a radiative core), little internal mixing occurs, resulting in a very dense and compact core. Contrarily, all three of the higher mass stars form convective cores due to the high luminosity and temperature gradients. These convective cores mix material efficiently, leading to nearly uniform distribution throughout. The lack of mixing in radiative cores causes steep, centrally peaked profiles, while the efficient mixing in convective cores produces flatter central regions.

In regards to temperature and radius, these results align as well:

Temperature and Radius Plots

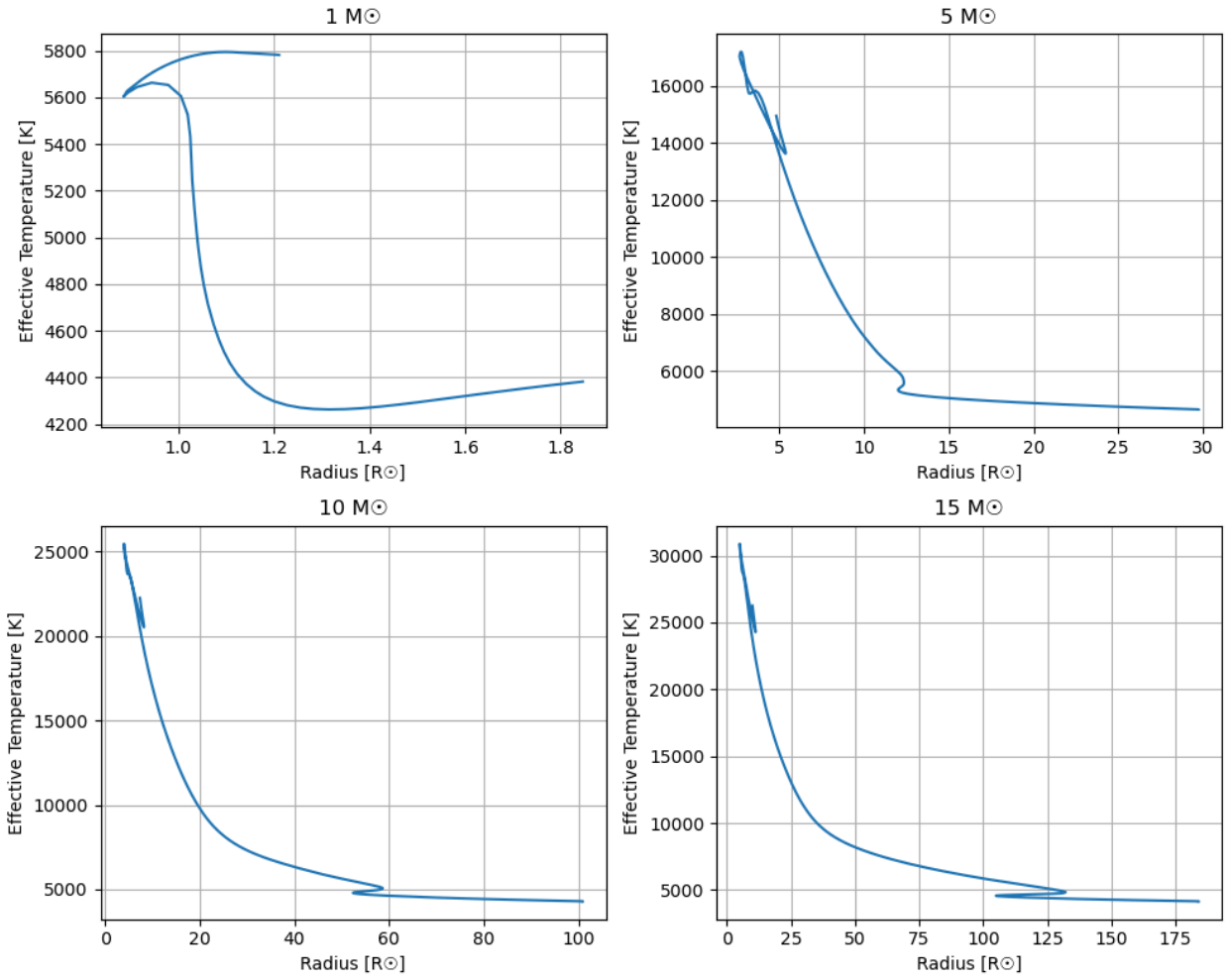

Figure 4. Effective temperature T_{eff} as a function of stellar radius R for the same four models. Temperature decreases outward through each star, consistent with radiative diffusion. The higher-mass models achieve larger radii and higher surface temperatures, reflecting CNO-cycle burning and radiation-pressure support, while the 1 $M_{\odot}$ model remains cooler and more compact, powered mainly by the p–p chain.

These temperature versus radius profiles reinforce the same mass-dependent trends seen in the density plots. Throughout each of the four plots, temperature decreases as radius increases, indicating that effective temperature is highest near the stellar core and dwindles outward toward the surface. The inverse correlation between temperature and radius is expected and reflects the

luminosity equation $L = 4\pi R^2 \sigma T^4$. For a roughly constant luminosity during the main sequence, any increase in radius must be accompanied by a substantial decrease in temperature, as reflected in the trials as well as the theory.

The magnitudes of the axes and maximums of the curves further strengthen the dependency of stellar structure on mass. The low mass star of $1\ M_\odot$ maintains a relatively moderate surface temperature of around 5800 K. This matches the behavior of small mass stars as they generate energy primarily through the p–p chain, which operates at lower core temperatures and luminosities. In the graph, this activity leads to fewer changes in R and T_{eff} over the main sequence as compared to the higher mass stars. These higher mass stars of $5\ M_\odot$, $10\ M_\odot$, and $15\ M_\odot$ reach temperatures and radii many orders larger than that of the $1\ M_\odot$ star. According to theory, higher mass stars mainly generate energy through the CNO cycle, which requires extremely high temperatures to maintain equilibrium, paralleling the temperatures observed in the trials.

Finally, the relationship between metallicity and time also corresponds to the earlier findings:

Metallicity and Time Plots

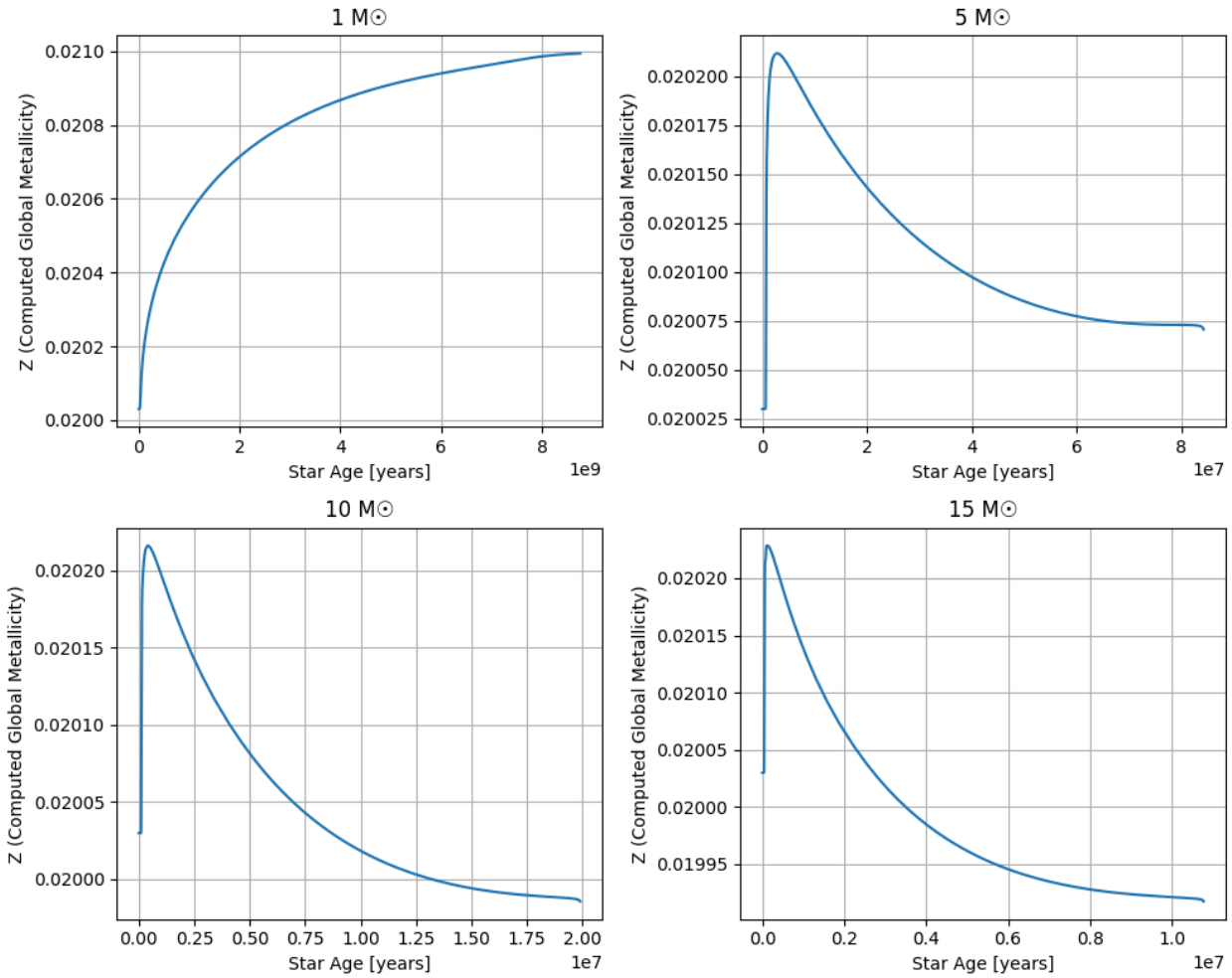

Figure 5. Evolution of the global, mass-averaged metal mass fraction $Z = 1 - (M_H + M_{He})/M_{star}$ for $1\ M_\odot$, $5\ M_\odot$, $10\ M_\odot$, and $15\ M_\odot$ models. The brief early spike corresponds to pre-main-sequence relaxation, while the slow rise thereafter reflects hydrogen depletion and helium enrichment. Higher-mass stars evolve more rapidly and display larger short-term composition changes due to convective mixing and faster hydrogen burning.

The above figures shows the evolution of the computed global, mass-averaged metal mass fraction, $Z = 1 - (M_H + M_{He})/M_{star}$, for four stars of masses $1\ M_\odot$,$5\ M_\odot$,$10\ M_\odot$, and $15\ M_\odot$ where M_H and M_{He} are the total hydrogen and helium masses within the star at each

timestep. All of the trials demonstrated a steep early rise at the start of the tracks, near the zero-age main sequence, followed by a slowing approach towards an asymptotic value for the rest of the main-sequence. The lower mass star, $1\ M_{\odot}$, evolves on much longer timescales than the higher mass stars, and shows only a small change in Z over its lifetime. This trend indicates a steady conversion of hydrogen to helium in the core, with little mixing because energy transport in lower mass stars is dominated by radiative diffusion and they lack large convective cores, leading to a slowing increase in Z over time. Conversely, the $5\ M_{\odot}$, $10\ M_{\odot}$, and $15\ M_{\odot}$ models display a sharp, short-lived spike in Z right at the beginning of their tracks but fall more quickly towards their plateaus. These trends fall in line with theoretical expectations. Stellar structure theory predicts that higher-mass stars burn hydrogen much faster and have shorter lifetimes, so composition changes driven by core hydrogen converting to helium occur earlier for larger masses. The early spike most likely corresponds to pre-main sequence relaxation and internal mixing as the model settles into hydrostatic and thermal equilibrium, rather than genuine heavy element production. The longer, slowing decline reflects continual hydrogen burning (which increases the helium fraction and thus reduces the computed residual because of helium's higher mass) and convective mixing in the larger mass stars, which redistributes newly formed elements within both the core and envelope, smoothing out composition.

Conclusion

My primary objective for this project was to explore how stars of different initial masses evolve using MESA and to compare the results of these simulations to theoretical predictions from stellar astrophysics. To test whether MESA reproduces the expected evolutionary behaviors

across the mass spectrum, I analyzed H–R diagrams, density–radius plots, metallicity evolution, and central temperature–density relations for stars of $1\ M_{\odot}$, $5\ M_{\odot}$, $10\ M_{\odot}$, and $15\ M_{\odot}$.

My findings confirm that MESA accurately predicts the trends projected by stellar theory. Low mass stars remain cool and dense with minimal core enrichment, while massive stars rapidly reach high central temperatures and enrich their cores through successive burning stages. The evolutionary paths through all of my diagrams matched theoretical expectations.

Works Cited

MESA Instrument Papers and Documentation. (n.d.). *Modules for Experiments in Stellar Astrophysics (MESA)*. Retrieved from https://docs.mesastar.org

Paxton, B., Bildsten, L., Dotter, A., Herwig, F., Lesaffre, P., & Timmes, F. (2011). Modules for Experiments in Stellar Astrophysics (MESA). *The Astrophysical Journal Supplement Series, 192*(1), 3. https://doi.org/10.1088/0067-0049/192/1/3

Paxton, B., Cantiello, M., Arras, P., Bildsten, L., Brown, E. F., Dotter, A., Mankovich, C., Montgomery, M. H., Stello, D., Timmes, F. X., & Townsend, R. H. D. (2013). Modules for Experiments in Stellar Astrophysics (MESA): Planets, Oscillations, Rotation, and Massive Stars. *The Astrophysical Journal Supplement Series, 208*(1), 4. https://doi.org/10.1088/0067-0049/208/1/4

Paxton, B., Marchant, P., Schwab, J., Bauer, E. B., Bildsten, L., Cantiello, M., Dessart, L., Farmer, R., Hu, H., Langer, N., Townsend, R. H. D., Townsley, D. M., & Timmes, F. X. (2015). Modules for Experiments in Stellar Astrophysics (MESA): Binaries, Pulsations, and Explosions. *The Astrophysical Journal Supplement Series, 220*(1), 15. https://doi.org/10.1088/0067-0049/220/1/15

Paxton, B., Schwab, J., Bauer, E. B., Bildsten, L., Blinnikov, S., Duffell, P., Farmer, R., Goldberg, J. A., Marchant, P., Sorokina, E., Thoul, A., Townsend, R. H. D., Wolf, W. M., & Timmes, F. X. (2018). Modules for Experiments in Stellar Astrophysics (MESA): Convective

Boundaries, Element Diffusion, and Massive Star Explosions. *The Astrophysical Journal Supplement Series, 234*(2), 34. https://doi.org/10.3847/1538-4365/aaa5a8

Paxton, B., Smolec, R., Schwab, J., Gautschy, A., Bildsten, L., Cantiello, M., Dotter, A., Farmer, R., Goldberg, J. A., Jermyn, A. S., Kanbur, S. M., Marchant, P., Pedersen, M. G., Thoul, A., Townsend, R. H. D., Wolf, W. M., & Timmes, F. X. (2019). Modules for Experiments in Stellar Astrophysics (MESA): Pulsating Variable Stars, Rotation, Convective Boundaries, and Energy Conservation. *The Astrophysical Journal Supplement Series, 243*(1), 10. https://doi.org/10.3847/1538-4365/ab2241

Prialnik, D. (2009). *An Introduction to the Theory of Stellar Structure and Evolution* (2nd ed.). Cambridge University Press.